BULLETIN OF THE POLISH ACADEMY OF SCIENCES
TECHNICAL SCIENCES, Vol. 60, No. 4, 2012
DOI: 10.2478/v10175-012-0095-5

Influence of the stator winding resistance on the field-weakening operation of the DRFOC induction motor drive

K. NGUYEN-THAC, T. ORLOWSKA-KOWALSKA*, and G. TARCHALA

Wroclaw University of Technology, 19 Smoluchowskiego St., 50-372 Wroclaw, Poland

Abstract. In this paper, an analysis of the influence of the stator winding resistance on the field-weakening operation of the induction motor drive based on the Direct Rotor Flux Oriented Control (DRFOC) is presented. Two scenarions of the optimal field-weakening algorithm (with and without stator winding resistance taken into account) have been compared and verified through simulation and experiment, under different operation conditions of the DRFOC drive system with 3 [kW] induction motor.

Key words: induction motor, optimal field-weakening, direct field oriented control.

List of symbols

$i_{\max}$	–	maximum stator current magnitude
i_s, i_{sx}, i_{sy}	–	stator and $x-y$ axis current components
i_{sA}, i_{sB}, i_{sC}	–	stator phase current components
$u_{\max}$	–	maximum stator voltage magnitude
$u_s, u_{sx}, u_{sy}, u_{dc}$	–	stator, $x-y$ axis components and DC bus voltage
$u_{s\alpha}, u_{s\beta}$	–	$\alpha-\beta$ axis components of stator voltage
m_e, m_L	–	electromagnetic and load torque
ω_s, ω_m, ω_r	–	stator, rotor and slip angular frequency
ψ, ψ_r	–	main and rotor flux
r_s, r_r	–	stator and rotor winding resistance
x_s, x_r	–	stator and rotor winding self-reactance
x_M	–	main reactance
$\sigma = 1 - x_M^2/x_s x_r$	–	total leakage factor
S_A, S_B, S_C	–	state functions of transistor branch
$(\mathbf{u}, \mathbf{i}, \boldsymbol{\psi})$	–	vector value
Subscript $\ldots_N$	–	rated value
Subscript $\ldots_b$	–	value at base speed
Subscript $\ldots_c$	–	value of a critical speed
Subscript $\ldots_{lim}$	–	limit values
Superscript...*	–	reference values
Superscript $\ldots^{opt}$	-	optimal values
Superscript...^	–	estimated values

All variables and parameters, written in small letters, are in per-unit system [p.u.]. Base values, necessary for the transition, can be found in [1].

1. Introduction

An induction motor (IM) thanks to its well-known advantages, such as simple construction, reliability, ruggedness and low cost has found a very wide range of industrial applications also including recently traction drives. Furthermore, in contrast to the DC motor, it can be used in dust and explosive atmosphere since there are no problems when using IM in industrial drives with high performance demands. Due to the developed frequency control methods, IM drives recently have substituted effectively the DC motor drives in industry.

The IM control methods can be divided into scalar and vector control [1, 2]. In the scalar control, which is based on relations valid for steady states, only magnitude and frequency (angular speed) of voltage, current and flux linkage space vectors are controlled. Thus, the control system does not act on the positions of the space vectors during transients. On contrary, in vector control, which is based on the relations valid for dynamic states, not only magnitude and frequency but also instantaneous positions of voltage, current and flux space vectors are controlled. According to the above definition, vector control is a general control philosophy that can be implemented in many different ways.

In the cases of closed loop controlled voltage-source inverter (VSI) fed IM drives, the vector method based on the rotor flux oriented control (RFOC) with direct or indirect current control is the most used scheme. It can be regarded as a matured technique for various applications [1–4]. However, in many applications, electrical drives have to deliver a constant torque (rated or maximum) at low speed only, and to decrease the torque and operate at almost constant power at medium and high speeds. In these cases, weakening of the motor flux (field weakening – FW) is a suitable control method which results in an economic rating of the power converter and motor.

The most frequently applied method of the FW control adjusts the excitation level of the machine by feed-forward control in inverse proportion to the mechanical speed of the motor. However, the 1990s showed renewed interest in the optimal methods for the FW control of IMs [5–7]. For rotor-flux orientation it was shown that the classical FW method of selecting the flux-producing current component proportional to

*e-mail: teresa.orlowska-kowalska@pwr.wroc.pl

the rotor speed inverse, yields too large current value, and a maximum torque is not achieved [7, 8]. Various strategies for improved FW operation were proposed [9–11]. As the control of the IM flux is obtained indirectly by controlling the motor current, the algorithm presented in [11] (a related scheme was proposed in [10]) for achieving the maximum torque is rather complex, requires tuning of several PI regulators (two PI regulators are used for current regulation, two PI regulators for FW and another one for speed regulation).

In the 2000s, several improved techniques were proposed [12, 13]. The foregoing schemes discussed two FW regions, with base and critical speed set-point (ω_{sb}, ω_{sc}), but the influence of the stator winding resistance on those set-points has not been previously investigated.

In this paper there is presented the following issue: the influence of the stator winding resistance on the speed set-points, as well as the flux and torque current components is analyzed, based on the optimal DRFOC scheme for IM control in the whole speed range, including the FW region. Increasing influence of r_s due to the reduction of the DC link voltage of the voltage-source inverter is especially taken into account. Such a behavior is typical for electric or hybrid vehicles because their DC voltage is supplied by a battery bank, so the DC link voltage will vary from 70% to 100% of nominal voltage.

2. Speed control regions of the induction motor

The operating speed range of the IM drive can be divided in three sub-regions: constant torque region ($\omega_s < \omega_{sb}$), constant power region ($\omega_{sb} \leq \omega_s < \omega_{sc}$), and constant slip frequency region ($\omega_s \geq \omega_{sc}$) [2], as it is shown in Fig. 1.

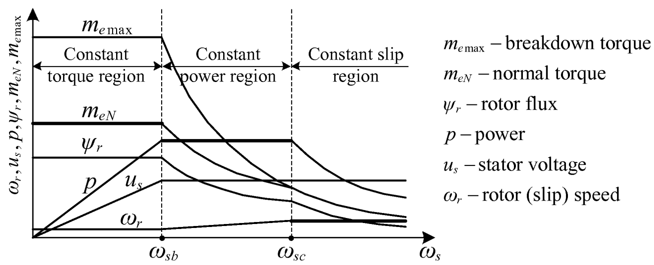

Fig. 1. Control characteristics of the induction motor in constant and weakened flux regions

The base and critical speeds are very important set-points, because they decide when the FW algorithm has to be applied to obtain a proper control of the IM.

In Fig. 2 two wrong choices of the base speed are shown. In Fig. 2a ω_{sb} is too small, so the FW begins too early and maximum torque is reduced; and on the contrary – by applying the FW too late (i.e. ω_{sb} is too big), voltage limit is utilizing and there is no enough voltage reserve to produce required torque (see Fig. 2b).

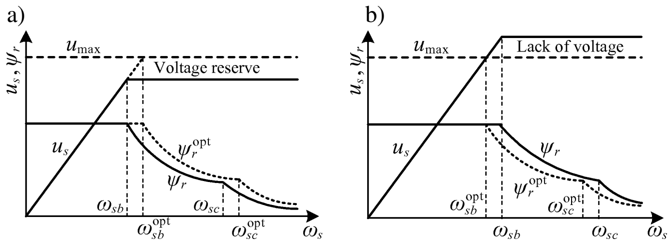

Fig. 2. Fig. 2. Wrong selection of the base speed set-point: a) too small base speed, b) too great base speed

Thus, the proper setting of the base and critical speeds is crucial in proper FW control of the IM drive. To solve this task, current and voltage limits, as well as stator resistance influence must be taken into account in control algorithms.

3. Current and voltage limits

The maximum torque of the IM is limited by the current and voltage ratings of the power inverter and thermal current limit of the IM. Therefore, it is useful to analyse performance of the machine under the current and voltage constraints in the $x-y$ synchronous reference frame [10], rotating with the angular field frequency $\omega_s = \omega_{s\psi}$.

The current constraint of the inverter can be expressed as follows (all expressions written in the paper are in per unit system [1]):

$$i_{sx}^2 + i_{sy}^2 \leq i_{\max}^2, \tag{1}$$

where $i_{\max} = \max(|\mathbf{i}_s|) = \max\left(\sqrt{i_{sx}^2 + i_{sy}^2}\right)$.

This relationship limits the current magnitude to the circle defined by $i_{\max}$.

The voltage constraint of the inverter is given as:

$$u_{sx}^2 + u_{sy}^2 \leq u_{\max}^2, \tag{2}$$

where $u_{\max}$ is set by the available voltage, which is a function of the pulse-width-modulation (PWM) strategy and the available DC-bus voltage (u_{dc}).

This equation indicates that the voltage magnitude $|\mathbf{u}_s| = \sqrt{u_{sx}^2 + u_{sy}^2}$ cannot exceed the ellipse defined by u_{max} and ω_s in (5). Nowadays, mainly the Space Vector Modulation (SVM) is used, thus $u_{\max}$ is limited in the linear region to $u_{dc} = \sqrt{3}$; however, overmodulation can provide $2u_{dc}/\pi$ [6].

The steady-state stator voltage equations of the IM are given directly from the motor mathematical model [1]:

$$u_{sx} = r_s i_{sx} - \omega_s \sigma x_s i_{sy}, \tag{3}$$

$$u_{sy} = r_s i_{sy} + \omega_s x_s i_{sx}. \tag{4}$$

The equation for the voltage limit ellipse (5) can be derived by substituting (3), (4) into (2) and (1):

$$\left(\frac{r_s i_{sy}}{u_{\max}} + \frac{x_s i_{sx}}{u_{\max}/\omega_s}\right)^2 + \left(\frac{r_s i_{sx}}{u_{\max}} - \frac{\sigma x_s i_{sy}}{u_{\max}/\omega_s}\right)^2 \leq 1 \tag{5}$$

When the stator resistance is neglected, equation (5) becomes a simple ellipse equation:

$$\left(\frac{x_s i_{sx}}{u_{\max}/\omega_s}\right)^2 + \left(\frac{\sigma x_s i_{sy}}{u_{\max}/\omega_s}\right)^2 \leq 1 \tag{6}$$

In case of the rotor flux oriented control of the IM, rotor flux and torque can be described as follows [10]:

$$\psi = \psi_r = \psi_{rx} = x_M i_{sx}, \tag{7}$$

$$m_e = \frac{x_M}{x_r}\psi_r i_{sy} = \frac{x_M^2}{x_r} i_{sx} i_{sy}. \tag{8}$$

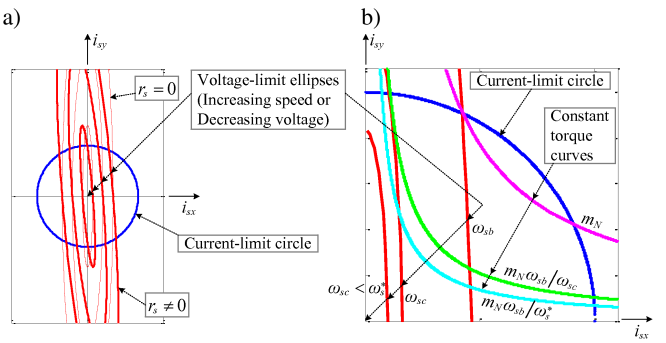

Fig. 3. General form of current-limit circle (1) and voltage-limit ellipse (5) and (6) – (a); detailed of Fig. 3a with investigated data of the induction machine and some constant torque curves (8) – (b)

Figure 3a shows a general form of the current limit circle and voltage limit ellipses; the dashed line ellipses are constraints when the stator resistance is neglected, in contrast – the bold line ellipses are the constraints when the stator resistance is included. The major effect of the stator resistance is to rotate the ellipse counter clockwise. The centre of the voltage limit ellipse is the origin, which implies that as the frequency increases or voltage decreases, the voltage constraint will shrink toward the origin (see denominators in the equation (5) and (6)).

4. Field-weakening algorithms and influence of the stator resistance

The FW algorithm should provide the robust and stable current regulation in the whole speed range, including FW region, by making sure that the IM is operated within the voltage and the current maximum constraints. Under the assumption of the slow enough variation of the rotor flux and the precise vector control, the current maximizing the torque (8) of the IM, can be derived from the constraints given by (1), (2) and (5). The possible operating region is the inside area of the current circle and voltage ellipse and the torque is depicted as a reciprocal proportion curve in the current plane, as shown in Fig. 3.

4.1. Constant torque region ($\omega_s \le \omega_{sb}$). If the i_{sx} current for the maximum torque, which is the current at the crossing point of the ellipse and the circle, is larger than its rated value i_{sxN}, it should be set as the rated value to prevent the magnetic saturation of the IM. That is the case of point B$_1$ in Fig. 4, where the torque m_{e1} may be obtained with i_{sx1}, but larger than i_{sxN} and it would result to cause saturation of the magnetic circuit of the IM. In this case, reference flux current i_{sx}^*should be set as i_{sxN}:

$$i_{sx}^* = i_{sxN} = \psi_{rN}/x_M \tag{9}$$

and the operating point should be B in the Fig. 4, generating torque m_{e2}.

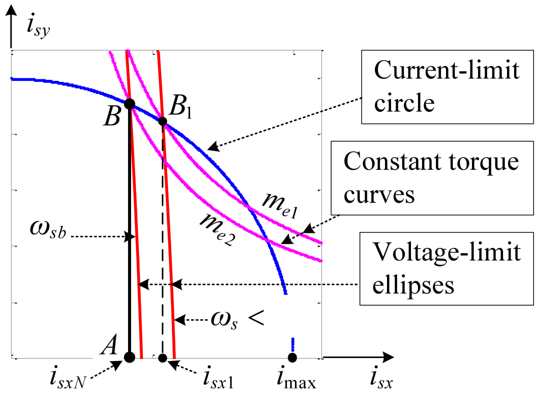

Fig. 4. Constant torque region

Also, the maximum available torque is dependent only on the maximum value of the torque current component $i_{sy\,\lim}^*$, which is given by the current constraint (10):

$$i_{sy\,\lim}^* = \sqrt{i_{\max}^2 - i_{sxN}^2} \quad \text{or} \quad i_{sy}^* \le \sqrt{i_{\max}^2 - i_{sxN}^2} \tag{10}$$

and the maximum torque is always the same as m_{e2} in this region. Hence, the region is called the constant torque region. In this region, the operating point should lie on the A-B line in the Fig. 4 with generating maximum torque m_{e2} (at point B).

Thus, the rotor flux reference value can be calculated as follows:

$$\psi_r^* = \psi_{rx}^* = x_M i_{sx}^*. \tag{11}$$

As the speed increases and the side of the ellipse decreases, the circle coincides with the nominal current, i_{sxN}. The angular frequency, where the constant torque operation region ends is defined as the stator base frequency, ω_{sb}. It can be obtained from (5) as follows:

$$\omega_{sb} = \frac{\sqrt{u_{\max}^2(i_{sxb}^2+\sigma^2 i_{syb}^2) - r_s^2(i_{sxb}^2+\sigma i_{syb}^2)} - (1-\sigma) r_s i_{sxb} i_{syb}}{\left(i_{sxb}^2+\sigma^2 i_{syb}^2\right) x_s}, \tag{12a}$$

where $i_{sxb} = i_{sxN}$ – base flux current component, $i_{syb} = \sqrt{i_{\max}^2 - i_{sxb}^2}$ – torque current component at base speed.

Thus, equation (12a) can be written in the following form:

$$\omega_{sb} = \frac{1}{x_s}\sqrt{\frac{u_{\max}^2 - r_s^2}{i_{sxN}^2(1-\sigma^2) + \sigma^2 i_{\max}^2}} - \frac{(1-\sigma^2)\, r_s i_{sxN}\sqrt{i_{\max}^2 - i_{sxN}^2}}{x_s\,(i_{sxN}^2\,(1-\sigma^2) + \sigma^2 i_{\max}^2)}. \tag{12b}$$

When neglecting the stator resistance, the base speed becomes:

$$\omega_{sb}\big|_{r_s=0} = \frac{u_{\max}}{x_s\sqrt{i_{sxN}^2(1-\sigma^2) + \sigma^2 i_{\max}^2}}. \tag{13}$$

Simultaneously, the mechanical base speed, ω_{mb}, can be obtained from:

$$\omega_{mb} = \omega_{sb} - \omega_{rN}, \tag{14}$$

where ω_{rN} is the nominal angular slip frequency.

4.2. Constant power region ($\omega_{sb} < \omega_s \leq \omega_{sc}$) **– FW region I.** In this operation region, when the machine delivers the rated power, the torque production will be inversely proportional to the speed:

$$m_e = \frac{x_M^2}{x_r} i_{sx} i_{sy} \sim \frac{1}{\omega_m} \cong \frac{1}{\omega_s}. \tag{15}$$

This operation region starts from the base speed, ω_{sb}, and ends at a critical speed, ω_{sc}, above which there is no more crossing points between the ellipse (at ω_s^*) and the constant torque curve (at command torque value $m_e^* = m_N \omega_{sb} / \omega_s^*$) – see Fig. 5.

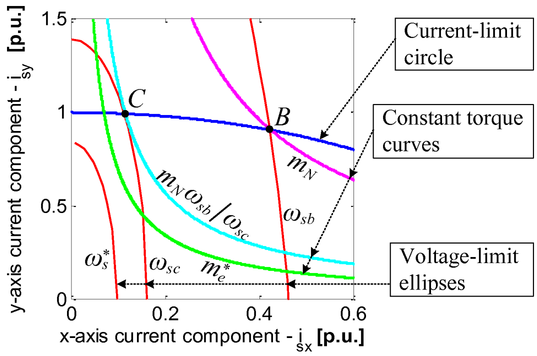

Fig. 5. Field-weakening region I

To obtain maximum torque in the FW region I, the operation point must lie on the B-C line, which is the intersection between the current limit circle, and the voltage limit ellipses. It can be seen in Fig. 5. When $\omega_s = \omega_{sc}$, the voltage limit ellipse and the constant torque curve (at $m_{ec} = m_N \omega_{sb} / \omega_{sc}$) intersect each other at only one point (contact point C).

Thus, the command currents (i_{sx}^*, i_{sy}^*) for maximizing the motor torque can be obtained as (16) and (18) while equating (1), (2) and (5):

$$i_{sxFWI}^* = \sqrt{(A-B)/C}, \tag{16}$$

where

$$A = x_s \omega_s \left(\begin{array}{l} u_{\max}^2 (\sigma+1) - \sigma^2 i_{\max}^2 (\sigma+1) x_s^2 \omega_s^2 + \\ + (1-3\sigma) r_s^2 i_{\max}^2 \end{array} \right),$$

$$B = 2 r_s \sqrt{\begin{array}{l} \left((\sigma^2+1) x_s^2 \omega_s^2 + 2 r_s^2 \right) u_{\max}^2 i_{\max}^2 - \\ - \left(x_s^2 \omega_s^2 \sigma + r_s^2 \right)^2 i_{\max}^4 - u_{\max}^4 \end{array}},$$

$$C = x_s \omega_s (1-\sigma) \left((\sigma+1)^2 x_s^2 \omega_s^2 + 4 r_s^2 \right).$$

When neglecting the stator resistance, the reference flux current (16) becomes:

$$i_{sxFWI}^* \big|_{r_s=0} = \frac{\sqrt{u_{\max}^2 - \omega_s^2 x_s^2 \sigma^2 i_{\max}^2}}{\omega_s x_s \sqrt{1-\sigma^2}}, \tag{17}$$

$$i_{syFWI\,\lim}^* = \sqrt{i_{\max}^2 - i_{sx}^{*2}} \quad \text{or} \quad i_{syFWI}^* \leq \sqrt{i_{\max}^2 - i_{sx}^{*2}}. \tag{18}$$

Simultaneously, the rotor flux command can be obtained from (11).

In this region, the slip angular frequency is increased as the speed increases. While the speed is further increased, the slip reaches the maximum value due to the voltage limit and then the FW region II begins. The angular slip value for maximum (break down) torque is given by the following expression .[1, 2]:

$$\begin{cases} \omega_{r\max} = \dfrac{r_r \sqrt{\omega_s^2 x_s^2 + r_s^2}}{\sqrt{(\sigma \omega_s x_r x_s)^2 + r_s^2 x_r^2}}, \\ \omega_{r\max}\big|_{r_s=0} = \dfrac{r_r}{\sigma x_r}. \end{cases} \tag{19}$$

A comparison of maximum slip angular frequencies in two cases: with and without stator resistance included, is presented in Fig. 6, as a function of the stator frequency. In this figure, minimum DC voltage is assumed as $0.7 u_{dcN}$, therefore the minimum critical speed takes the value $\omega_{sc\min} = 1.77$ [p.u.] and thus at this set-point the difference in $\omega_{r\max}$ is about 0.4% of $\omega_{sc\min}$. At higher speeds this difference is reduced.

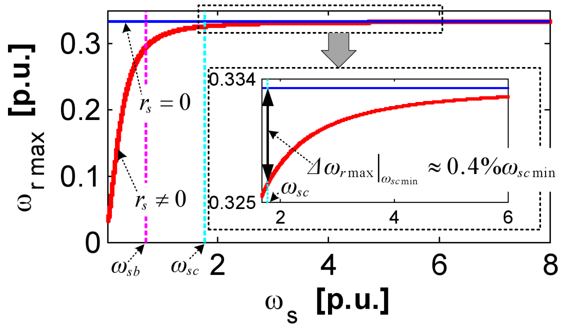

Fig. 6. Maximum slip angular frequency with and without stator resistance included

4.3. Constant slip region ($\omega_s > \omega_{sc}$) **– FW region II.** As the speed and angular slip frequency are further increased, the stator operating frequency is also increased, and the voltage limit ellipse is more reduced (see (5) and (6)), and its large portion begins to be included in the circle shown in Fig. 7. The onset of region II, ω_{sc}, is the time when for the optimal current values (pointsin line C-D in the Fig. 7) for given maximum torque only the voltage limits is the constraint to be considered. Thus, the torque is maximized if and only if $|u_{sx}| = |u_{sy}| = u_{\max}/\sqrt{2}$ [14].

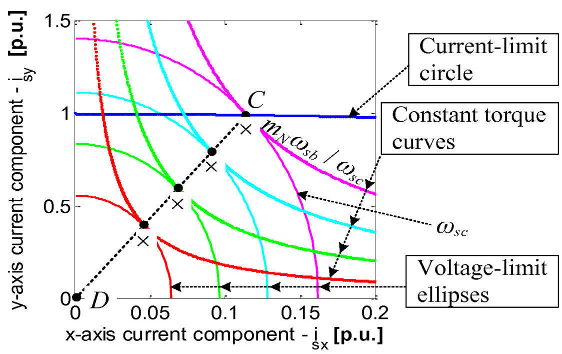

Fig. 7. Field-weakening region II

Therefore, the optimal current components for the maximum torque can be obtained as (20), (21):

$$\begin{cases} i^*_{sxFWII} = \dfrac{u_{\max}\left(\omega_s \sigma x_s - r_s\right)}{\sqrt{2}\left(r_s^2 + \omega_s^2 \sigma x_s^2\right)}, \\ i^*_{sxFWII}\big|_{r_s=0} = \dfrac{u_{\max}}{\sqrt{2}\omega_s x_s}, \end{cases} \tag{20}$$

$$\begin{cases} i^*_{syFWII\ \lim} = \dfrac{u_{\max}\left(\omega_s x_s + r_s\right)}{\sqrt{2}\left(r_s^2 + \omega_s^2 \sigma x_s^2\right)}, \\ i^*_{syFWII\ \lim}\Big|_{r_s=0} = \dfrac{u_{\max}}{\sqrt{2}\omega_s \sigma x_s} \end{cases} \tag{21}$$

and rotor flux command as (11).

The critical speed is the only one solution of multi-equation (1), (2), (5) and (8) with $m_e = m_N \omega_{sb}/\omega_{sc}$:

$$\omega_{sc} = \frac{\sqrt{\begin{array}{l} u_{\max}^2 + \sqrt{u_{\max}^4 + 8\sigma K u_{\max}^2} + 4\sigma K + \\ +\sigma^2 u_{\max}^2 + \sigma^2 \sqrt{u_{\max}^4 - 8K u_{\max}^2} - 4\sigma^2 K \end{array}}}{2\sigma x_s i_{\max}}, \tag{22}$$

where $K = r_s x_s x_r m_N \omega_{sb}/x_M^2$

$$\omega_{sc}\big|_{r_s=0} = \frac{u_{\max}\sqrt{2\left(\sigma^2+1\right)}}{2\sigma x_s i_{\max}}. \tag{23}$$

5. Influence of the stator resistance on speeds and reference currents

Next, the detailed influence of the stator winding resistance on allowable values of the reference stator current components is investigated. In Fig. 8 the differences of the flux current component in the FW regions of investigated IM (see for parameters in Sec. 6) in two cases of limit conditions are presented (region I – in the left hand side and region II – in the right hand side). In Fig. 8a – for $u_{\max} = 1.0$ [p.u.], and $i_{\max} = 1.5$ [p.u.], the corresponding speeds $\omega_{sb} = 0.963$ [p.u.] and $\omega_{sc} = 2.5$ [p.u.]. Respectively – in Fig. 8b – for $u_{\max} = 0.7$ [p.u.], and $i_{\max} = 1.5$ [p.u.], the corresponding speeds $\omega_{sb} = 0.69$ [p.u.] and $\omega_{sc} = 1.765$ [p.u.].

Figure 8 shows, that in the FW region I, as the speed is increased, a relative difference caused by r_s inclusion (see lines (d) in the left-hand sides of Fig. 8a) also increases. The an opposite phenomenon is observed in the FW region II. On the other hand, the relative difference is much bigger when $u_{\max}$ is reduced (i.e. ω_{sb}, ω_{sc} are reduced); this increase is close to 20% in the FW Region II (see line (d) in Fig. 8b).

In Fig. 9 the speed set-points as functions of the limit conditions $u_{\max}$ and $i_{\max}$ are presented, according to equations (12) and (22), depending on the stator resistance. It can be seen that the FW region I is reduced in case without stator resistance ($r_s = 0$) (i.e. $\omega_{sb}|_{r_s \neq 0} < \omega_{sb}|_{r_s=0}$ and $\omega_{sc}|_{r_s \neq 0} > \omega_{sc}|_{r_s=0}$); especially the difference in the base speed is significant.

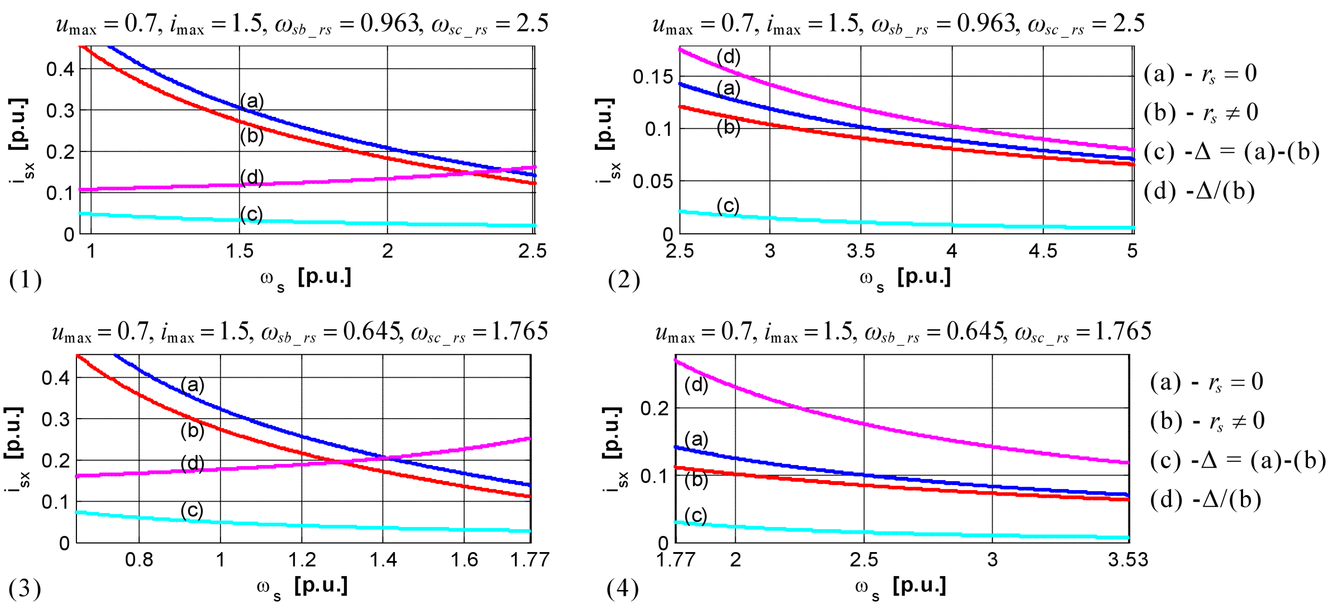

Fig. 8. Influence of the stator resistance on reference values of the flux current components for $i_{\max} = 1.5$ [p.u.] and: (1) FW region I and (2) FW region II with $u_{\max} = 1.0$ [p.u.], (3) FW region I and (4) FW region II with $u_{\max} = 0.7$ [p.u.]

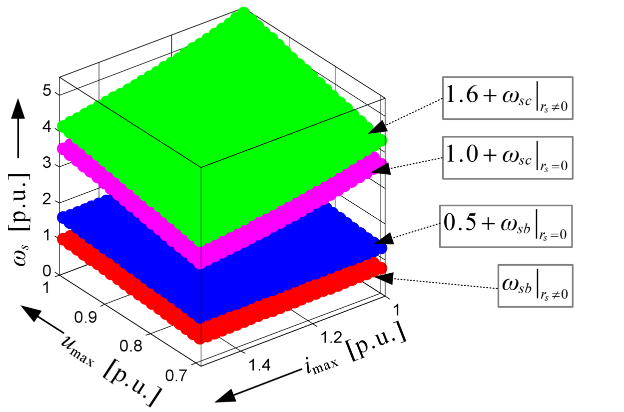

Fig. 9. Influence of the stator resistance on base and critical speeds

6. Control system implementation

The analysed FW algorithm has been implemented in the DR-FOC structure [1] with the Space Vector Pulse Width Modulation method for the Voltage Source Inverter [15] and tested in simulation and experiment. The classical flux reference look-up table is replaced by the optimal flux reference, calculated according to the voltage and current limits, and the new block diagram is presented in Fig. 10.

All simulation and experimental tests were realized for the IM with following rated data: $P_N = 3.0$ [kW], $n_N = 1400$ [rpm], and following per-unit parameters of the equivalent circuit: $r_s = 0.0707$, $r_r = 0.0637$, $x_s = x_r = 1.9761$, $x_M = 1.8780$. In the tests, the all variables and set-points are in per-unit system ([p.u.]).

6.1. Simulation results. In the following figures chosen simulation and experiment results for tests of the FW algorithms with and without stator resistance effect are presented and compared. All the tests with the same conditions of voltage and current limit: $u_{dc} = 0.6$, $u_{\max} = 0.35$, $i_{\max} = 1.5$.

In Fig. 11 simulation results for the first FW region, for two cases with and without stator resistance under the same conditions: $m_L = 0.215$ and $\omega_m^* = 0.5$ are demonstrated.

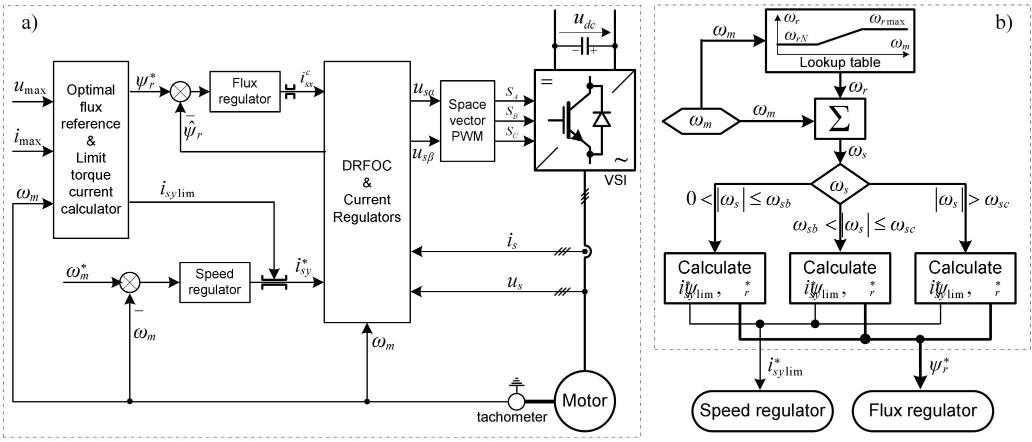

Fig. 10. Block diagram of the DRFOC with optimal FW strategy (a) and the optimal flux reference algorithm scheme (b) (with and without r_s included)

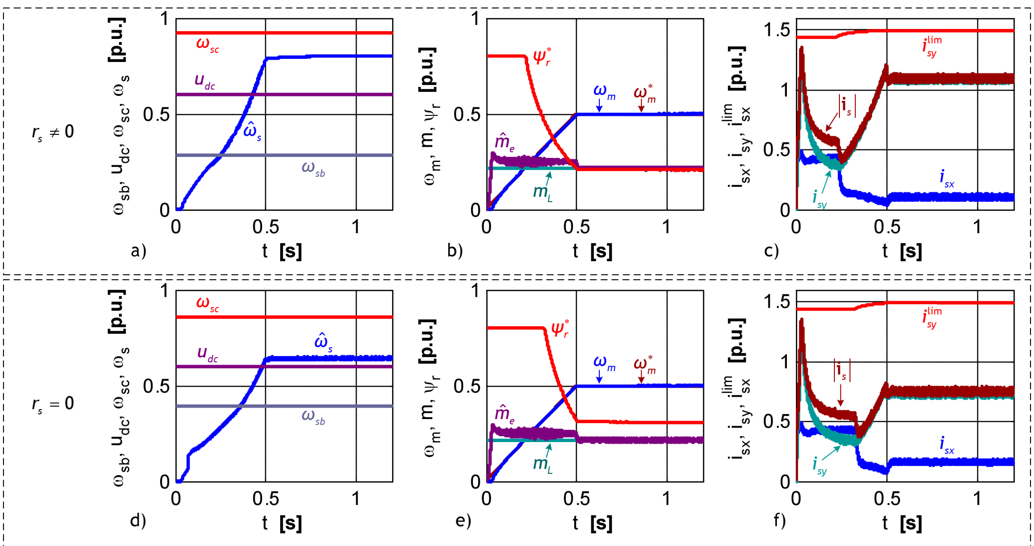

Fig. 11. Simulation results for the FW region I: (a, b, c) with r_s and (d, e, f) without r_s ($u_{\max} = 0.35$, $i_{\max} = 1.5$, $m_L = 0.215$ and $\omega_m^* = 0.5$)

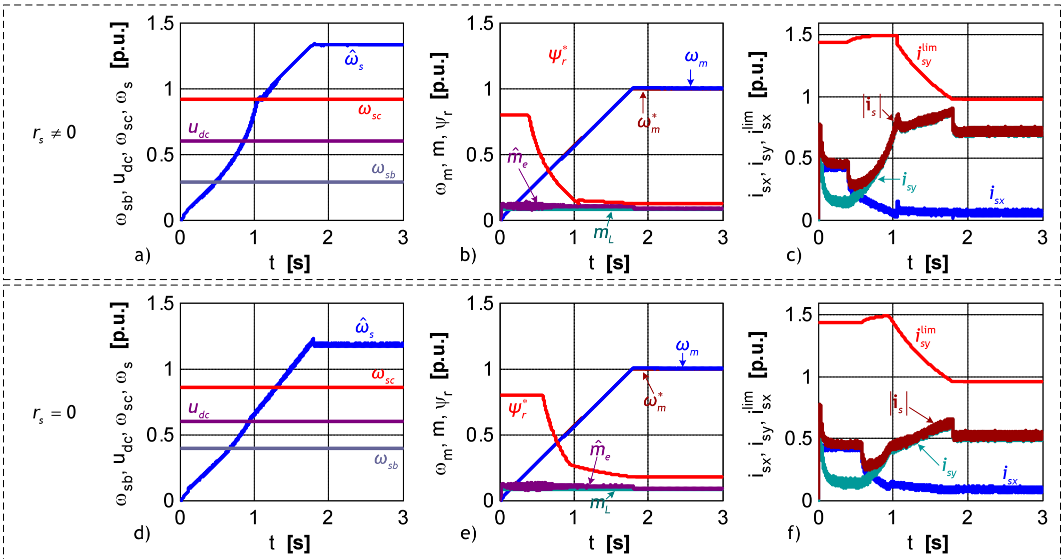

Fig. 12. Simulation results for the FW region II: (a, b, c) with r_s and (d, e, f) without r_s ($u_{\max} = 0.35$, $i_{\max} = 1.5$, $m_L = 0.085$ and $\omega_m^* = 1.0$)

In Fig. 12 simulation results for the second region of the FW for two cases with and without stator resistance under follow conditions: $m_L = 0.085$ and $\omega_m^* = 1.0$ are presented.

Simulation results in Figs. 11 and 12 show that, in the case of r_s included in all equations, the flux current component (i_{sx}) and rotor flux (ψ_r) values are smaller than without r_s taken into account. Thus, with the same load torque, the torque current component (i_{sy}) in the case with r_s should be bigger than without r_s case, according to (8).

In the FW region I, the voltage and current reserve is enough, so the limit of the torque current component $i_{sy}^{\lim}$ is about $i_{\max}$ (see Fig. 11c, f). In contrast, when motor operates in the FW region II, the limit of the torque current component is only warranted by the voltage constraint, therefore it will be smaller than maximum current set-point ($i_{\max}$) – see Fig. 12a, f.

6.2. Experiment results. The theoretical considerations were confirmed experimentally. The laboratory set-up, presented in Fig. 13 is composed of the 3 [kW] induction motor driven by the static converter. The motor is coupled to a load machine by a stiff shaft. The control and FW algorithms are implemented with a digital signal processor using the dSPACE hardware and software.

Similar to the simulation conditions, the voltage and current limits in the experimental tests are: $u_{dc} = 0.6$, $u_{\max} = 0.35$, $i_{\max} = 1.5$.

In Fig. 14, experiment results for the first region of the FW for two cases, with and without stator resistance, under following conditions are presented: $m_L = 0.215$ and $\omega_m^* = 0.5$.

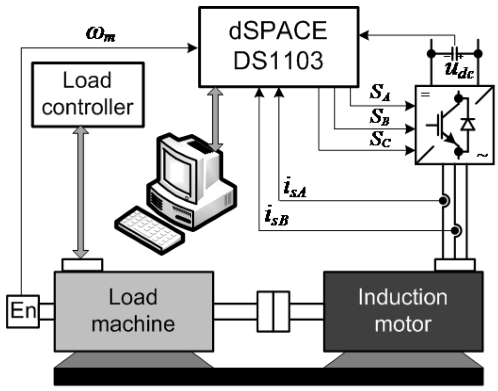

Fig. 13. Schematic diagram of the laboratory test bench

In the first region of FW tests, the same results are obtained as in the simulation: in $r_s \neq 0$ case, the flux current component (or rotor flux) is smaller than for $r_s = 0$ case, on contrary to the torque current component (see Fig. 14 b, c, e, f). Therefore, slip speed in $r_s \neq 0$ case is bigger, so estimated synchronous speed ($\widehat{\omega}_s$) is bigger than in $r_s = 0$ case (see Fig. 14a, d).

In next Fig. 15 experimental results obtained for the higher reference speed $\omega_m^* = 1.0$ and load torque $m_L = 0.085$ are shown. Similar to the simulation results, in a steady state of the second FW region, the flux current components (i_{sx}) of $r_s \neq 0$ case is deeply reduced according to (20) and a generated torque current component is higher ($i_{iy} \approx i_{sy}^{\lim}$ – see Fig. 15c). Meanwhile, the torque current component in $r_s = 0$ case is much lower than limit value. Therefore, the estimated synchronous speed in the $r_s \neq 0$ case is much bigger than in the $r_s = 0$ case (see Fig. 15a, d).

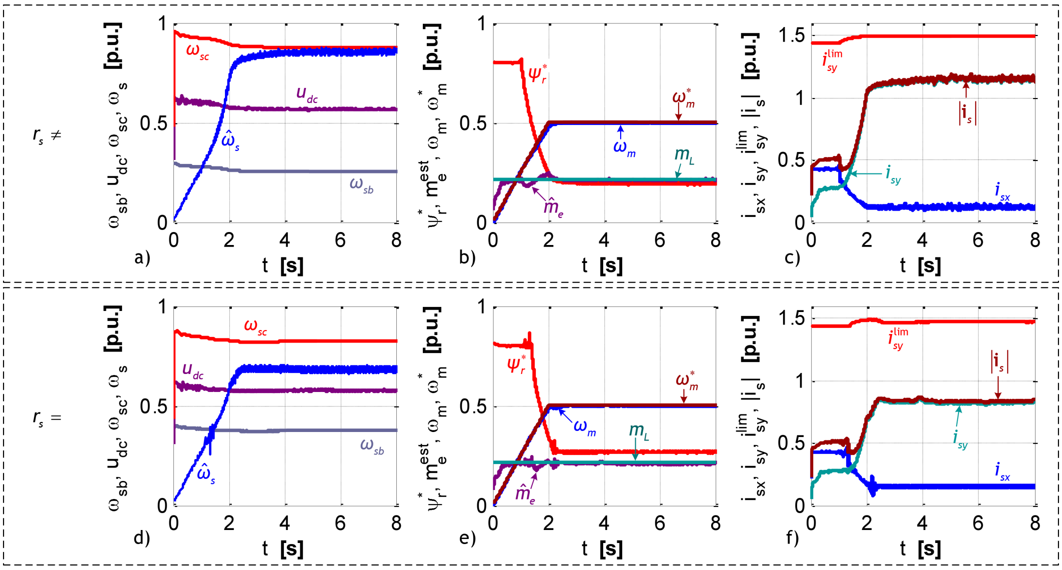

Fig. 14. Experimental results for the FW region I: (a, b, c) with r_s and (d, e, f) without r_s ($u_{dc} = 0.6$, ($u_{\max} = 0.35$), $i_{\max} = 1.5$, $m_L = 0.215$ and $\omega_m^* = 0.5$)

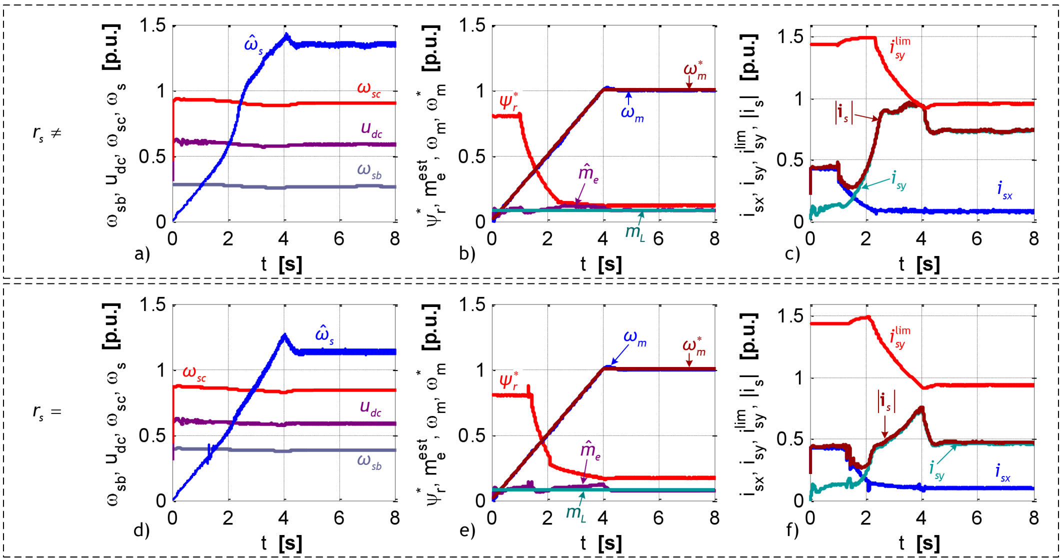

Fig. 15. Experimental results for the FW region II: (a, b, c) with r_s and (d, e, f) without r_s ($u_{dc} = 0.6$, ($u_{\max} = 0.35$), $i_{\max} = 1.5$, $m_L = 0.085$ and $\omega_m^* = 1.0$)

7. Conclusions

In this paper, considering the voltage and the current limits as well as the influence of the stator winding resistance on the FW operation of the DRFOC induction motor drive is analysed.

The optimal FW algorithm based on the machine mathematical model is discussed, as well as the importance of the stator resistance effect on the controlled stator current components in the FW operation region, especially in a low limit voltage case, is highlighted.

Simulation and experiment results for the DRFOC structure of the induction motor shows that the drive system is stable in the FW region if the stator resistance is taken into account, especially in the second FW range. When the stator resistance is considered, the flux is more reduced, at the same time the developed torque is also reduced.

REFERENCES

[1] T. Orlowska-Kowalska, *Speed Sensorless Induction Motor Drives*, Wrocław University of Technology Press, Wrocław, 2003, (in Polish).

[2] M.P. Kazmierkowski and H. Tunia, *Automatic Control of Converter-fed Drives*, Elsevier, London, 1994.

[3] M. Dybkowski, T. Orłowska-Kowalska, M.P. Kazmierkowski, and D. Stando, “Induction motor drive control in traction applications”, *Scientific Works Inst. of Electr. Mach., Drives and Meas. of Wroclaw Univ. of Tech.: Studies and Materials* 64 (30), 139–150 (2010).

[4] T. Orlowska-Kowalska and M. Dybkowski, "Performance analysis of the sensorless adaptive sliding-mode neuro-fuzzy control of the induction motor drive with MRAS-type speed estimator", *Bull. Pol. Ac.: Tech.* 60 (1), 61–70 (2012).

[5] X. Xu, R. de Doncker and D.W. Novotny, "Stator flux orientation control of induction machines in the field weakening region", *Proc. IEEE Ind. Appl. Society Annual Meet.* 1, 437–443 (1988).

[6] X.Y. Xu and D.W. Novotny, "Implementation of direct stator flux orientation control on a versatile DSP based system", *IEEE Trans. Ind. Appl.* 27 (4), 694–700 (1991).

[7] X.Y. Xu and D.W. Novotny, "Selection of the flux reference for induction machine drives in the field weakening region", *IEEE Trans. Ind. Appl.* 28 (6), 1353–1358 (1992).

[8] S.H. Kim and S.K. Sul, "Maximum torque control of an induction machine in the field weakening region", *IEEE Trans. Ind. Appl.* 31 (4), 787–794 (1995).

[9] H. Grotstollen and A. Bunte, "Control of induction motor with orientation on rotor flux or on stator flux in a very wide field weakening region – experimental results", *Proc. IEEE Int. Symp. Ind. Electr.* 2, 911–916 (1996).

[10] H. Grotstollen and J. Wiesing, "Torque capability and control of a saturated induction-motor over a wide-range of flux weakening", *IEEE Trans. Ind. Electr.* 42 (4), 374–381 (1995).

[11] S.H. Kim and S.K. Sul, "Voltage control strategy for maximum torque operation of an induction machine in the field-weakening region", *IEEE Trans. Ind. Electr.* 44 (4), 512–518 (1997).

[12] G. Gallegos-Lopez, F.S. Gunawan, and J.E. Walters, "Current control of induction machines in the field-weakened region", *IEEE Trans. Ind. Appl.* 43 (4), 981–989 (2007).

[13] L. Harnefors, K. Pietilainen, and L. Gertmar, "Torque-maximizing field-weakening control: design, analysis, and parameter selection", *IEEE Trans. Ind. Electr.* 48 (1), 161–168 (2001).

[14] K. Nguyen-Thac, G. Tarchala, and T. Orłowska-Kowalska, "Comparative analysis of the chosen field-weakening methods for the direct rotor flux oriented control drive system", *Archives of Electr. Eng.* 61 (4), 443–454 (2012).

[15] G. Radomski, "Control and modulation methods of voltage source converter", *Bull. Pol. Ac.: Tech.* 57 (4), 323–336 (2009).